Sediment Problems and Sediment Management in Asian River Basins
(Proceedings of the Workshop held at Hyderabad, India, September 2009). IAHS Publ. 349, 2011.

Spatially-distributed assessment of sediment yield and shallow landslide potential area in the upper Citarum River basin, Indonesia

APIP[1], KAORU TAKARA[2] & YOSUKE YAMASHIKI[2]

1 *Graduate School of Urban and Environment Engineering, Kyoto University, Kyoto 615-8540, Japan*
apip@flood.dpri.kyoto-u.ac.jp

2 *Disaster Prevention Research Institute (DPRI), Kyoto University, Uji 611-0011, Japan*

Abstract Frequently, only a few locations within a basin are critical and responsible for high amounts of soil loss due to surface soil erosion and shallow landslide events. In connection with sediment yield reduction programmes, effective control of soil losses requires implementation of best management practices (BMPs). For the effective and efficient implementation of BMPs, identification of such critical locations is essential. In this study a physically-based hydrological–geotechnical model was applied to an upland tropical basin, with the aim of providing an assessment tool for identification of critical sub-basins. The model consists of two primary components. These comprise a hillslope sediment–runoff component, which considers soil detachments by rain and surface runoff; and a stochastic slope instability algorithm. Daily streamflow and suspended sediment discharge data, as well as the spatial patterns of documented historical landslides, were used for model evaluation and application. Critical sub-basins were identified on the basis of spatially-distributed sediment yields and areas predicted as susceptible to shallow landsliding. The study demonstrated the high potential applicability of the proposed modelling approach for identifying areas vulnerable to erosion and thus important sediment sources.

Key words soil erosion; slope instability; sediment yield; distributed model; critical sub-basins; Citarum River, Indonesia

INTRODUCTION

The upper Citarum River basin, in West Java, Indonesia, was selected as a study area. The Saguling Dam was constructed at the outlet of the basin in 1986. The main purpose of this dam is to provide a main source of hydropower in Java Island, and also to supply water to freshwater fisheries and agriculture. Because of its position as the upper dam, most of the gross storage has already been filled by the large amount of sediment deposited during flood events. If this sedimentation continues, without prevention and control measures, the life of the dam will be limited and its functions restricted. The condition of the upper river basin is an important factor in controlling its hydrological response, including floods, soil erosion, landsliding, and sediment input to the Saguling Dam.

The upper Citarum River basin is recognised as an area with some of the most persistently active landslides in Indonesia. The floods that trigger the landslides occur almost every year and cause extensive damage. The hydrologic response of the basin has been changed by land degradation (Agus *et al*., 2003), and as a result, floods, debris flows and others landslide types are very frequent during the rainy season. The soils derived from volcanic tuff are highly erodible and prone to landslides. Hillslope erosion is also a serious problem in this upper area, where hillsides are steep. Shallow landsliding, as a form of mass wasting, and surface soil erosion are the main source of the basin sediment yield. Therefore, there was an urgent need to devise control measures.

Within sediment risk and disaster reduction programmes, effective control of sediment mobilisation requires implementation of BMPs in the critical sediment source areas of the basin. Numerous studies have indicated that, for many basins, a few critical locations are responsible for a high proportion of the downstream sediment load (Dickinson *et al*., 1990; Lin *et al*., 2008). Therefore, it is better to implement control and management measures in the most critical internal locations, as identified at the sub-basin scale, which makes it essential to prioritize individual sub-basins. Such prioritization involves ranking of the different critical sub-basins of a basin according to the order in which they should be targeted for the implementation of structural or non-structural control measures.

Research on identification of critical areas inside a basin on the basis of spatially-distributed sediment yields and the location of potential areas of shallow landsliding has to date not been widely reported in the literature. In addition, the Citarum River basin lacks a good network of gauging stations for hydrological, soil erosion, and landslide monitoring. Against this background, the main purpose of this contribution is to report the initial application of an integrated physically-based distributed hydrological–geotechnical model that can be used to predict soil erosion and sediment transport, as well as to assess land-surface susceptibility to landsliding within the basin. These model outputs are then used as a basis for identifying the main sub-basins responsible for sediment production.

Rainfall induced soil erosion and shallow landslides are the main sources of sediment supply in hilly basins such as the upper Citarum basin. These processes are generally modelled separately; an erosion model is used to predict soil loss, and a landslide model is used to assess slope failures and mass wasting. Therefore, this study hypothesized that applying a physically-based distributed hydrological–geotechnical model, which would share basic hydrological information, would result in integrated and improved prediction of hydrological response, erosion and sediment transport, and shallow landsliding. The model simulates the internal behaviour of the basin by taking into account the local topography and many other spatially-distributed factors, including rainfall, soil properties, and land use. However, if the model is complex and the basin scale is large, computational inefficiency can prove a drawback and limit the application of the model. To overcome these problems, this study also applied a new method for lumping a distributed soil erosion model.

STUDY AREA

The Citarum River is of vital importance for West Java Province and Jakarta City, Indonesia, in terms of economic development and the prosperity of the people. This study focused on the upper Citarum River basin, with the Saguling Dam as the outlet. The total area of the upper basin is the 2310 km^2 lying between 600 and 3000 m, and comprising 16 main sub-basins. Geographically, the area is located between 107°26′E–107°95′E and 6°73′S–7°25′S. The average gradient derived using a 90 m resolution DEM ranges from 0.01^o in the central area to 31.15° in the northern and southern parts (Fig. 1).

The current water related problems are floods and landslides in the wet season and droughts in the dry season. The hillslope areas of this region have been periodically exposed to hazards from shallow landslides and debris flows. Most of those landslides were triggered by a sequence of heavy rainfall events. The climate conditions are characterized by tropical monsoon with two distinct wet and dry seasons. Records from a local climatological station indicate that the period of heaviest rainfall extends from the beginning of November until December, and is followed by a second peak in March–April linked to the West Asian monsoon. The rainfall then quickly reduces during the period May–October due to the dry season associated with the East Asian monsoon. The annual rainfall for the study area ranges from 1500 mm up to 4000 mm, with almost 80% falling between November and April.

The nature of vegetation on the land surface influences both the hydrologic conditions and slope stability. Land use information was derived from LANDSAT7/ETM+ (30 m resolution) satellite images verified by field investigations. A 12-type land-use classification was applied for 2002 and 2005. Below 800 m, the land use is mainly paddy fields and settlement areas. At intermediate altitudes and on the steep slopes the land use is mainly farmland (cultivation of annual or tree crops), orchards (perennial trees), forest, grass, and shrub. Urbanized areas are also found on the steep slopes, although these are relatively small and are concentrated in several small areas which are highly susceptibility to landsliding.

The underlying geology consists mainly of Quaternary volcanic rocks with some Miocene sedimentary facies, granite, granodiorite, diorite, alluvium, Pleistocene volcanic facies, and Miocene limestone facies (Takeuchi *et al*., 1995). Due to the influence of the active volcano, the

soil types in the study area are varied and complex. Based on the digitized soil map and information on soil properties provided by FAO-UNESCO, the humic and ochric andosol soils are found mainly in the mountainous area, which was influenced by volcanic eruptions. Latosols are found along the Lembang fault, and alluvial soils occupy the side of the river valley. Soil thickness in the study basin ranges from less than 10 to 150 cm.

The basin has a limited spatial coverage of ground-based raingauges. The rainfall was measured by 17 daily raingauges and information on rainfall intensity was only available for one automatic recording station. Water level recorders were installed to measure streamflow discharge which was obtained using rating curves. These stations include one suspended sediment monitoring station located at the inlet of the Saguling Dam (Nanjung Station). The locations of these hydrological stations are shown in Fig. 1(b).

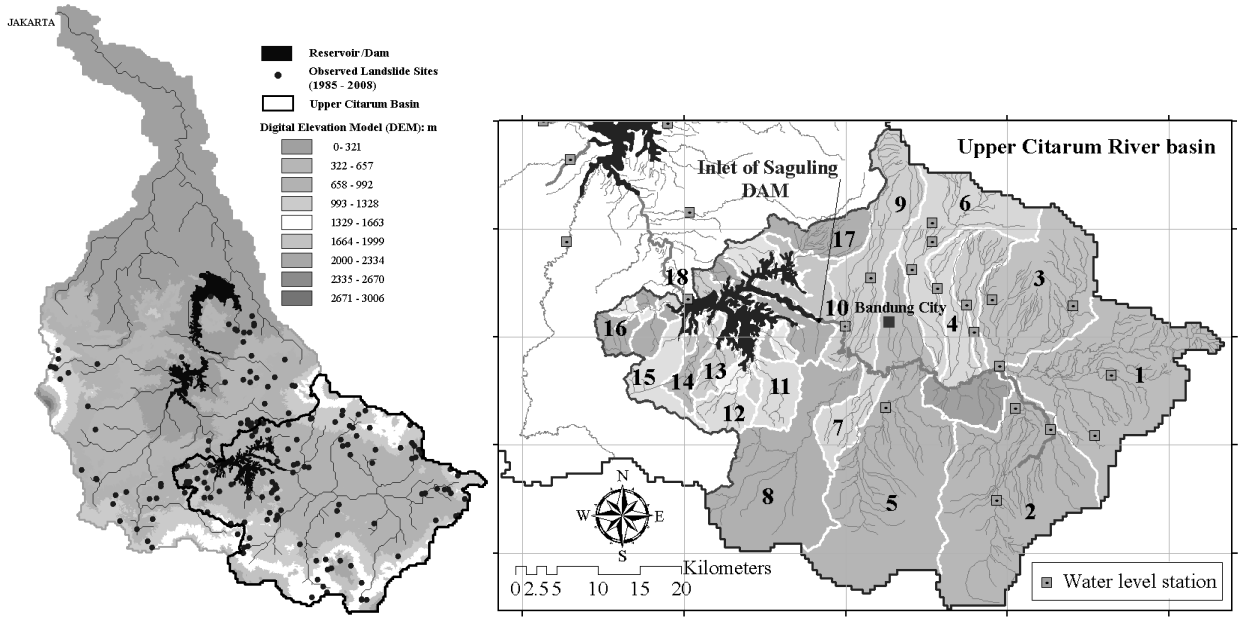

Fig. 1 (a) Location of the upper Citarum River basin and the DEM for the whole Citarum River basin. The filled circles indicate the locations of landslides as recorded by the Geological Agency of Indonesia. (b) Sub-basin boundaries (shown by numbers) and the location of water level stations.

OBSERVED SEDIMENT YIELDS AND LANDSLIDES

The upstream area of the Citarum basin is surrounded by many mountains, such as Mount Wayang, Mount Calancang, Mount Patuha, Mount Malabar, and Mount Tangkuban Perahu. Therefore, the upstream land area is steeply sloping. This situation is highly conducive to soil erosion and landsliding, if the land lacks a good vegetation cover and is poorly managed.

To provide information on soil erosion and landslide occurrence in the upper Citarum basin, the record of annual suspended sediment yield for the Nanjung Station and landslide inventory data for 1974–2008 are presented in Fig. 2(a). With an average flow of 92.3 $m^3 s^{-1}$, the mean annual suspended sediment yield for the period 1974–2008 was approx. 2.9 million t $year^{-1}$. With a reduction in vegetation cover within the upstream area after 1986, the sediment load increased to 6.80 million t $year^{-1}$ in 1992. Human impact has caused the sediment load to progressively increase over the 20-year period. Figure 2(a) also shows the annual distribution of landslide occurrence. These data suggest that the trend for increased annual sediment loads reflects the similar trend in the total number of landslide events each year. The seasonal distribution of sediment supply and landslide events during this period are plotted in Fig. 2(b). A very clear correlation between the climatic conditions and sediment supply as well as landslide incidence can now be observed. It

appears that high sediment loads and frequent landslides often occur during the rainy season, which extends from November until April, in association with a series of river flood events.

The landslides that occur in the study area can be classified into two types with regard to depth and speed of movement and overall risk. The first type comprises deep and slow landslides, which are in general relatively safe for people, since they allow evacuation even during periods of movement. However, landslide movement can be sufficient to destroy houses and other buildings and to cause large areas of damage. The second type comprises shallow and rapid landslides. These are dangerous, especially when many landslides can occur during the same triggering rainfall event, causing casualties and extensive damage to infrastructure. The speed of this type of landslide is very rapid and can involve rock, soil, and debris flows.

As example, three significant debris flow events occurred, those categorized come from rapid and shallow landslides triggered by heavy rainfall as follows: (1) landslide disaster in West Java at Cililin, Walahir village on 21 April 2004 that caused the death of at least 15 people, 43

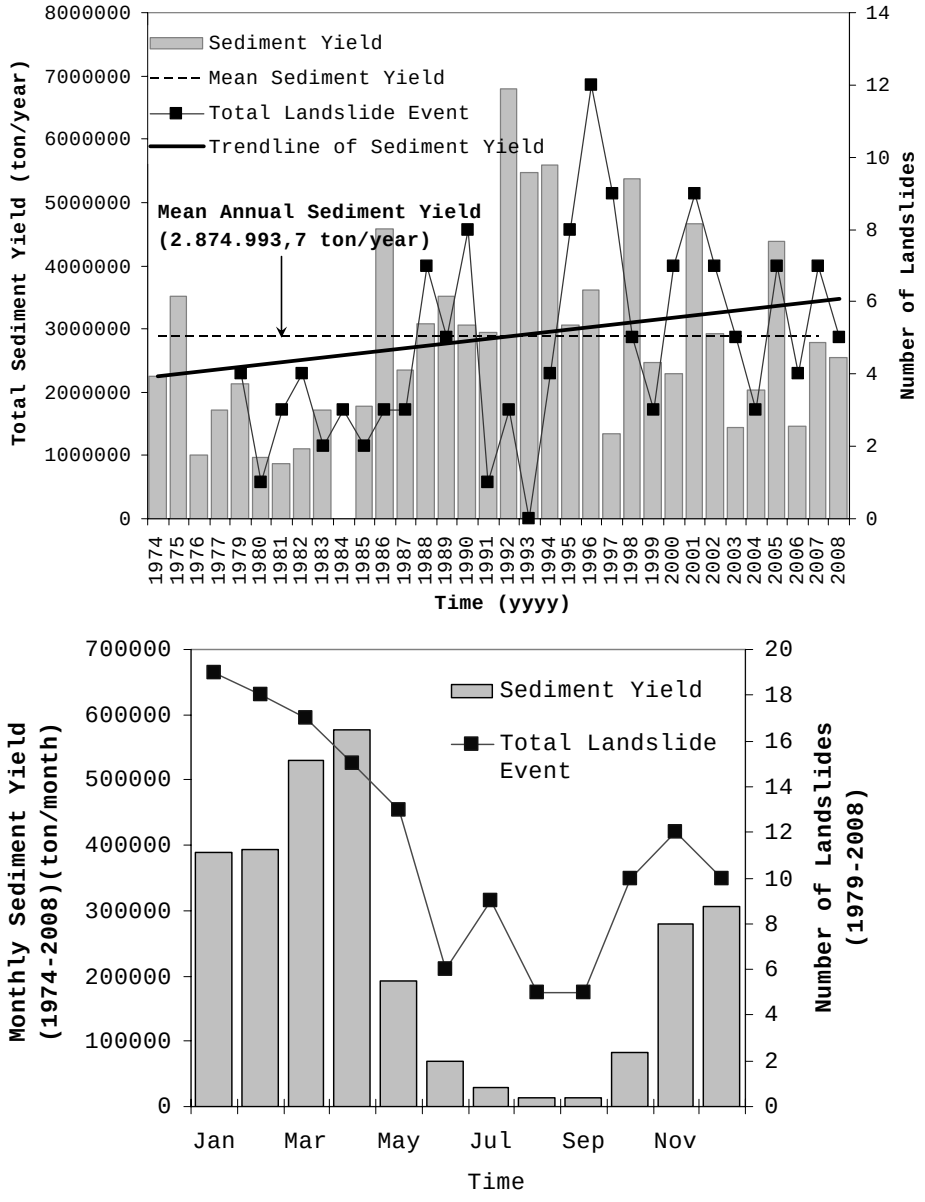

Fig. 2 (a) Annual distributions of sediment supply and frequency of landslide, and (b) seasonal variations of sediment supply and landslide frequency in the upper Citarum River basin.

houses collapsed or were badly damaged, and 60 ha of paddy fields were swept away by the landslides. This landslide mainly was due to heavy rainfall, steep slopes, high weathering products, and land-use change; and (2) landslides disaster in West Java at Pangalengan and Cikembang Villages on 15–16 March 2008 was believed to have caused the death of two residents and 48 houses were buried by the landslides. This landslide was mainly caused by heavy rainfall and steep slopes.

BASIC EQUATIONS OF THE INTEGRATED HYDROLOGICAL-GEOTECHNICAL MODEL

A recently developed physically-based hydrological–geotechnical model (Apip *et al*., 2010a,b) was used in this study. The model consists of hillslope hydrology, soil erosion, slope failure, and sediment transport algorithm. The hydrologic model was based on a kinematic wave approach and simulates three lateral flow mechanisms including subsurface and surface flows (Tachikawa *et al.*, 2004). The model simulates: (1) subsurface flow through capillary pores; (2) subsurface flow through non-capillary pores; and (3) surface flow on the soil surface. These three flow processes are represented by the following single set of stage–discharge relationships (equation (1)):

$$q = \begin{cases} v_m d_m (h_w / d_m)^{\beta}, & o \le h_w \le d_m \\ v_m d_m + v_a (h_w - d_m), & d_m \le h_w \le d_a \\ v_m d_m + v_a (h_w - d_m) + \alpha (h_w - d_a)^m, & d_a \le h_w \end{cases} \quad (1)$$

$$v_m = k_m i,\ v_a = k_s i,\ k_m = k_s / \beta,\ \alpha = \sqrt{i} / n,\ d_m = D\theta_m,\ d_a = D\theta_a$$

where q is discharge per unit width; h_w is water level; i is the topographic gradient; k_m is the saturated hydraulic conductivity of the capillary soil layer; k_s is the hydraulic conductivity of the non-capillary soil layer; d_m is the depth of the capillary soil layer; θ_m is the fraction of maximum volumetric water content in the capillary pore, d_a represents the depths of the capillary and non-capillary soil layers, θ_a is the fraction of maximum volumetric water content in the capillary and non-capillary pores; D is a soil depth; β is the exponent constant of unsaturated flow, v_m and v_a are the flow velocities of unsaturated and saturated subsurface flows, respectively, n is the Manning's roughness coefficient, which varies according to land-use type, and m is a constant.

Simulation of soil transport processes was also included in the above runoff model. Soil detachment processes associated with inter-rill and rill erosion are implicitly simulated as raindrop splash and surface flow detachment, respectively. The empirical equation of soil detachment by raindrops d_r is given as:

$$d_r = \mu\, k\, k_e = \mu\, k\, 56.48\, r \quad (2)$$

where μ is the soil erodibility; k is a parameter; and k_e is the total kinetic energy of the raindrops. The concept of sediment transport capacity was used to determine soil detachment or deposition by surface flow d_f (Foster, 1982):

$$d_f = \alpha\,(T_c - c) h_{ws} \quad (3)$$

where α is a proportionality coefficient; h_{ws} is the surface flow depth; c is the sediment concentration; and T_c is the maximum sediment concentration transport capacity, which determines soil erosion (when $T_c > c$) or deposition (when $T_c < c$). In the present work, the sediment transport capacity was calculated based on Unit Stream Power (USP) theory (Yang, 1996), and is expressed as:

$$T_c = \log\{i + j \log((vi - v_{critical}\ i) / \omega)\} \quad (4)$$

where vi is the unit stream power (where v is the surface flow velocity calculated by equation (1) and i is the slope gradient) and $v_{cr}i$ is the critical unit stream power for incipient motion, in which:

$$i = 5.435 - 0.386\log(\omega d_{50}/\upsilon) - 0.457\log(U^*/\omega)$$

$$j = 1.799 - 0.409\log(\omega d_{50}/\upsilon) - 0.314\log(U^*/\omega);\ \omega = F\left[gd_{50}\left(\frac{\rho_s}{\rho_w} - 1\right)\right]^{1/2}$$

where

$$F = \left[\frac{2}{3} + \frac{36\upsilon^2}{(\rho_s/\rho_w - 1)g\,d_{50}^{\,3}}\right]^{1/2} - \left[\frac{36\upsilon^2}{(\rho_s/\rho_w - 1)g\,d_{50}^{\,3}}\right]^{1/2}$$

where vi is the unit stream power (where v is the flow velocity and i is the slope gradient), $v_{critical}\,i$ is the critical unit stream power ($v_{critical}$ is the critical flow velocity), ω is the sediment fall velocity calculated by Rubey's equation, ρ_s is the sediment particle density, ρ_w is the water density, g is the specific gravity, d_{50} is the median grain size, and υ is the kinematic viscosity of the water. $U^*(=\sqrt{g\,i\,h_{ws}})$ is the average shear velocity. There are three model parameters that have to be calibrated μ, α, and d_{50}. A method of spatially lumping the distributed sediment–runoff model (Apip *et al*., 2010c) was used for spatially-distributed assessment of sediment yields at the sub-basin scale.

The infinite slope method of slope stability analysis, a physically-based approach, was adopted for assessment of probable shallow landslide locations. The potential slope failure algorithm has two functions: failure prediction and downslope mass re-distribution of sediment released from slope failures. The infinite slope methods determines the slope stability factor, i.e. the slope factor of safety (*FS*), which expresses the ratio of stabilizing to destabilizing forces. The criterion to decide whether a slope is unstable or stable depends upon the value of *FS* being smaller or larger than 1. In this study, *FS* is calculated using a method adopted by Borga *et al*. (2002), as presented in equation (5).

$$FS = \frac{c^* + \cos\theta\,[1 - r_w]\tan\phi}{\sin\theta};\begin{cases} c^* = \dfrac{c_r + c_s}{d_a\rho_s g + W} \\ r_w = \dfrac{h_w\rho_w}{\left(1 + \dfrac{W}{gd_a\rho_s}\right)d_a\rho_s} \end{cases} \tag{5}$$

in which c^* is the total cohesion (c_r+c_s), c_r and c_s are the effective root and soil cohesion; ϕ is the effective internal angle of the soil; W is the vegetation surcharge; d_a is the effective soil depth; h_w is the saturated height calculated using a hydrological algorithm; θ is the slope angle; ρ_s is the density of soil at field capacity; ρ_w is the density of water. Most of these terms are spatially variable, but it is assumed that only m (= h_w/d_a) is time-varying, and therefore, the factor of *FS* is a function of m. Assuming that the value of every term in equation (5), except for m, is known or can be estimated for each local area/grid cell, a critical relative saturation level for a grid, m^c, can be determined, where $m^c = FS^{-1}$ as follows:

$$m^c = \left(\frac{\rho_s}{\rho_w} + \frac{W}{gd_a\rho_w}\right)\left(1 - \frac{\tan\theta}{\tan\phi}\right) + \frac{c_r + c_s}{d_a\rho_w g\cos\theta\tan\phi} \tag{6}$$

Based upon the concept of critical soil saturation, three slope stability classes can be defined:

1. Theoretically always stable which is expressed by:

$$\tan\theta < \left(1 - \frac{1}{\dfrac{\rho_s}{\rho_w}\left(\dfrac{\rho_s}{\rho_w} + \dfrac{W}{gd_a\rho_w}\right)}\right)\tan\phi + \frac{c_r + c_s}{gd_a\rho_s\cos\theta\left(1 + \dfrac{W}{gd_a\rho_s}\right)} \tag{7}$$

2. Theoretically always unstable, which is expressed by:

$$\tan\theta \geq \left(\frac{c_r + c_s}{gd_a\rho_s \cos\theta\left(1 + \frac{W}{gd_a\rho_s}\right)} \right) + \tan\phi \tag{8}$$

3. Potentially stable or unstable. Slope instability analysis is undertaken only for those grid cells with slope stability classified as potentially "stable/unstable"with *FS* predicted by equation (5).

Land surfaces theoretically always stable are those predicted to be stable even when saturated. Slope elements theoretically always unstable are those predicted to be unstable, even under dry conditions. There are five model parameters that have to be calibrated c_r, c_s, W, ϕ, and ρ_s. To identify the critical sub-basins on the basis of the area susceptible to shallow landslides and to take account of the stochastic nature of the system, the Generalized Likelihood Uncertainty Estimation (GLUE) concept was adopted and incorporated into the above deterministic hydrological and slope stability algorithms to generate 10 000 landslide susceptibility maps. The procedures include a number of steps:

1. Generate a probabilistic distribution and sample the parameter space of each model parameter 10 000 times using a Monte Carlo simulation technique.
2. Measurement of model performance.
3. Define the criteria for acceptance or rejection of model results.

For each simulation, a grid cell with an *FS* value less than 1.0 is defined as a potential shallow landslide location, otherwise it is classified as stable. The long-term spatial pattern of recorded landslide locations (1985–2008) is overlaid on each susceptibility map. Two objective functions are used to measure the model performance for each susceptibility map, namely success rate in predicting unstable grid cells (OF1) and success rate in predicting unstable grid cells associated with success rate in predicting stable grid cells (OF2) (Huang & Kao, 2006). Accordingly, the cumulative probability of predicted landslides and a mean *FS* for each grid cell could be extracted; and thus a relative risk measure for landslide potential can be obtained. As a last stage, the probability of landslide potential, based on the slope instability index, is qualitatively classified as extremely low ($P \leq 0.2$), low ($0.2 < P \leq 0.4$), moderate ($0.4 < P \leq 0.6$), high ($0.6 < P \leq 0.8$), and extremely high ($0.8 < P \leq 1.0$).

MODEL APPLICATION

Sediment–runoff

Evaluation of the hydrological model performance was carried out through calibration and validation of the hydrological response, using long-term simulations. Adjustment of the final parameters was undertaken by performing Monte-Carlo-type simulations, on the basis of best model performance. The years 2004 and 2005 were selected as the calibration and validation periods. Sediment discharge data from the Nanjung Station was used to calibrate and validate the simulated streamflow discharges. The rainfall recorded at 17 daily rainfall stations, distributed in and around the basin, was utilized to account for the distribution of rainfall. However, only one recording (hourly) raingauge was available, and daily rainfall data were disaggregated to hourly values using an approach derived from analysis of the various temporal rainfall patterns of heavy rainfall events at the automatic raingauge located at the BMG Station. The total number of rainstorm events of different duration during the period 1986–2004 was analysed. We found that heavy 4-hour rainfalls represented the highest density of rainfall events. The average temporal distribution pattern of heavy 4-hour rainfalls was used as a simple model for generating hourly rainfall series from a daily rainfall. Then the hourly rainfall values were spatially interpolated. The spatial rainfall distribution in the basin was estimated using the Thiessen polygon method. The interpolated and disaggregated data standardized to a GIS format that served as the input for the

space- and time-varying hydrological model. The DEM was derived from HydroSHEDS products (http://hydrosheds.cr.usgs.gov).

Observed and simulated hydrographs and the cumulative sediment yield at Nanjung Station are summarized in Fig. 3, in which each panel shows the result of calibration and validation. Using the same parameters from the calibration period, the hydrological model was run for the validation period. The results depicted in Fig. 3 indicate that after calibration, the model yielded comparable results with respect to long-term daily streamflow and sediment discharges. The model generally predicted the overall shape of hydrographs and cumulative sediment yields reasonably well. The performance of the streamflow model was evaluated using the Nash-Sutcliff coefficient of efficiency (NSE). The NSE values for the calibration and validation periods resulted in high values (0.65–0.75), indicating that the model can effectively predict hydrological responses. The model satisfactorily reproduced the observed sediment yield at the Saguling Dam inlet, which was estimated to be about 1.0–2.7 million t year^{-1}.

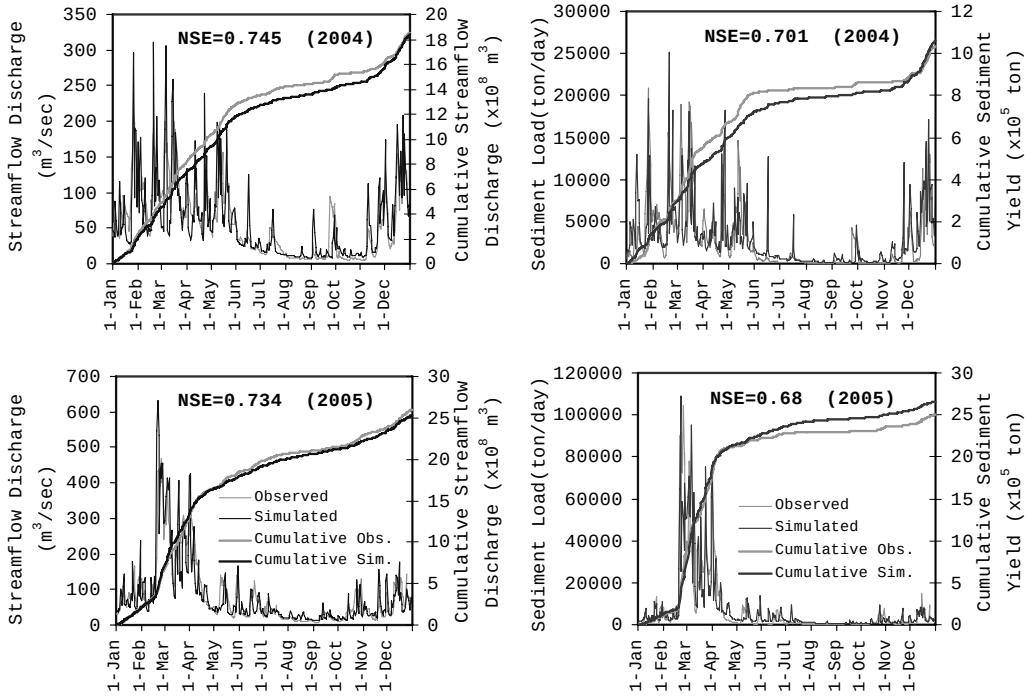

Fig. 3 Streamflow and sediment supply model performance for the calibration period 2004 (upper figures) and the validation period 2005 (lower figures). Streamflow and sediment discharges were evaluated at the upper basin outlet.

Shallow landslide susceptibility

Adjustment of the hydro-geomechanical parameters was conducted by performing Monte-Carlo-type simulation (MCS) and adopting the GLUE concept. Initial estimates for feasible ranges of the slope stability model parameters were based on field and laboratory measurements and the literature, as well as maps of soil types and soil thickness.

Following GLUE, we set a reference value for model performance (OF2 ≥ 0.50) to define the behavioural simulations. 2067 susceptibility maps were produced by applicable simulations. Here we demonstrate the advantage of using two objective functions; OF1 and OF2 to measure model performance and the problems of retrieving optimal model outcome. The 2067 top values of model performance derived from OF2 (*y*-axis) are plotted against the OF1 (*x*-axis) (Fig. 4). A dome-shape distribution is shown between the two objective functions. OF2-derived performance increases along with OF1-derived performance at the beginning. However, when OF2-derived

performance reaches a best prediction (0.64) and starts to decrease, OF1-derived efficiencies keep increasing until its best prediction (1.0) is reached. The result suggests that the OF2-derived performance helps to reduce over prediction. For further probability analysis, we overlay the maps and take the mean for *FS* values in each grid cell for the best 2067 predictions. The occurrence probability of $FS < 1.0$ for each grid cell is calculated for the 2067 runs to quantify predicted shallow landslide potential. Each grid cell has a mean *FS* value and an occurrence probability for shallow landsliding (Fig. 4).

Figure 5 shows the integrated landslide probability map derived from the best 2067 simulations and the spatial distribution of mean *FS*. Figure 5 demonstrates the pattern of areas predicted to be susceptible to shallow landslides, as described above, along with the general pattern of observed landslide sources. The model reproduced several of the principle clusters in the observed pattern, notably the clusters along an escarpment in the western, southern, eastern, and northern sectors of the basin. The percentage of basin area used to simulate the dynamic of susceptible areas to shallow landsliding in response to a rainfall event amounted to 32.1% (636 318 grid cells). Two types of error appeared in the predicted shallow landslide susceptibility map: (1) some grid cells were predicted as theoretically always stable, but past landslides were mapped in those grid cells, especially in the northern part of the study region; (2) some grid cells were characterized as zones of slope instability slope, but no scars were observed there. Such errors are typically caused by inaccuracies in the representation of topography. In steep terrain, the

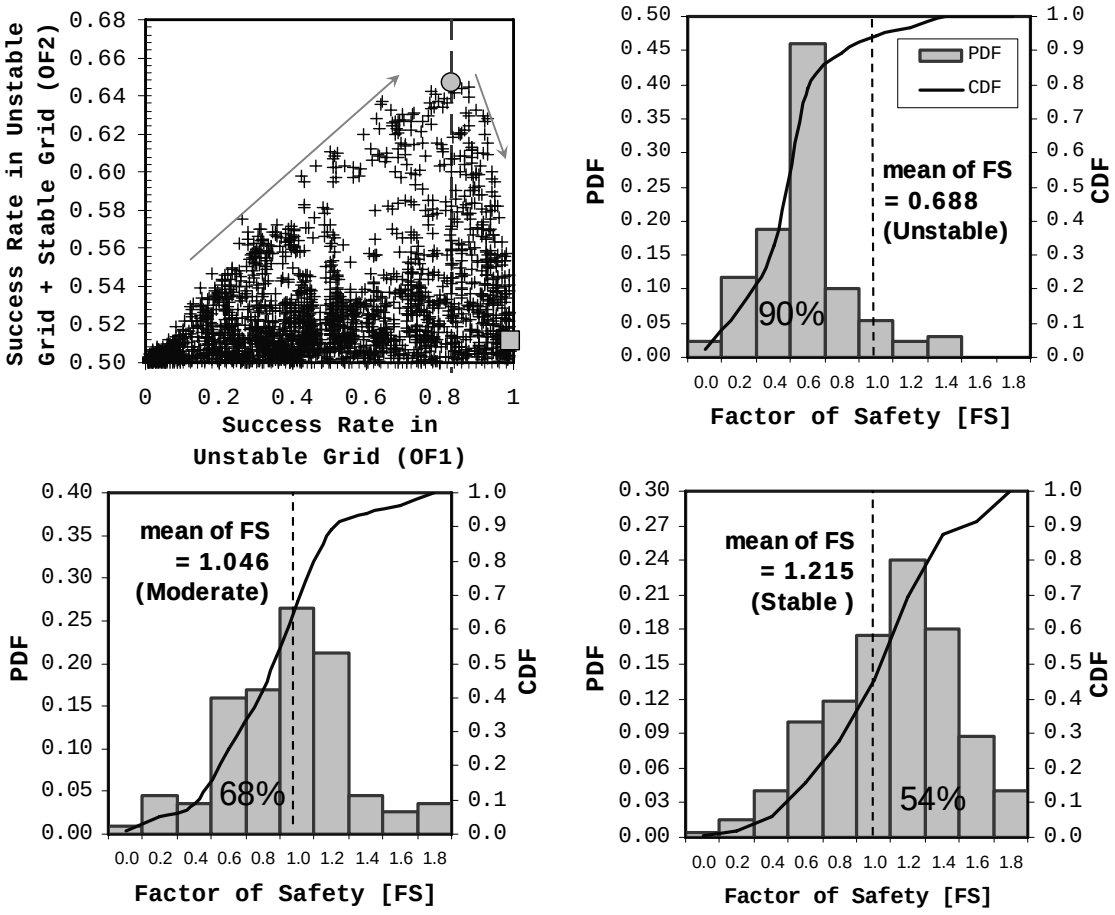

Fig. 4 The scatter plots of OF1 against OF3-derived efficiencies for 2067 runs (top, left column figure), and probability functions and their cumulative probability of the *FS* values in the three example grid cells with different mean *FS*: unstable (mean *FS* = 0.688); moderate (mean *FS* = 1.046); and stable (mean *FS* = 1.215).

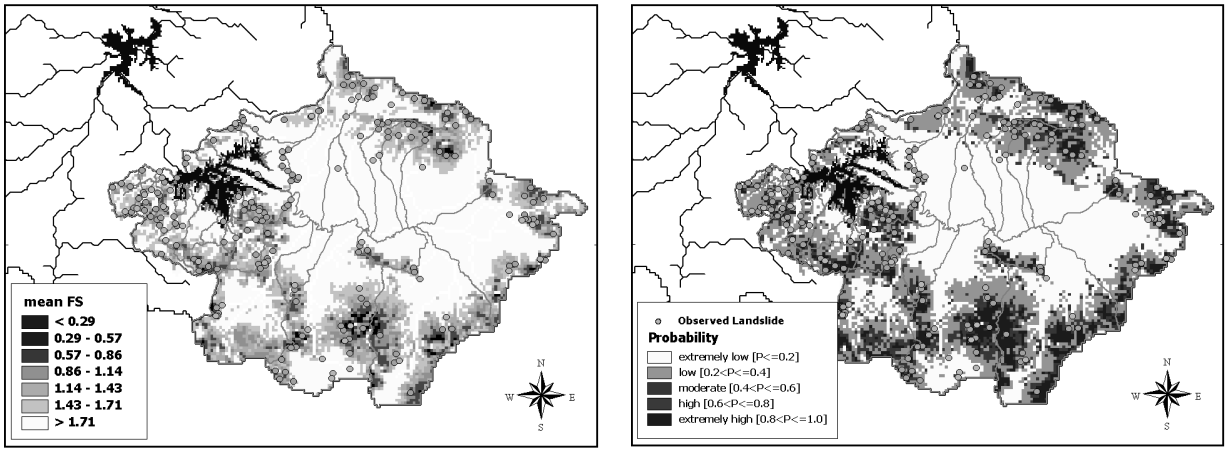

Fig. 5 The mean *FS* (left column) and integrated landslide probability map (right column) overlaid with the spatial distribution of observed landslide sites.

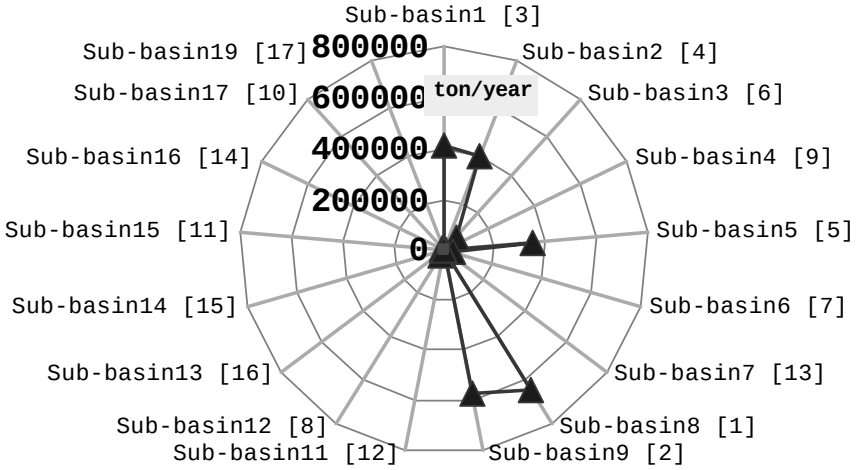

Fig. 6 Model output for identification of the critical sub-basins in the upper Citarum Basin. The ranking of critical sub-basins is shown by the number inside the brackets.

90-m grid DEMs provided by HydroSHEDS for particular internal locations still do not capture the local slope steepness that controls shallow landsliding. Consequently, the model did not represent local topographic controls on potential shallow landsliding.

IDENTIFICATION OF THE CRITICAL SUB-BASIN

According to the simulation results obtained for a wet year of 2001 (see Fig. 2(a)), the sub-basin where surface soil erosion and sediment productions were serious could be identified. On the basis of higher annual sediment yield, the sediment supplies from each sub-basin show that most sediment was generated and transported from sub-basins number 8, 9, 2, 1 and 5 (see Fig. 6). The annual sediment yields in these sub-basins were found to be critical. After arranging the critical sub-basins in ascending order, considering the sediment fluxes and yields from each sub-basin, potential priorities were fixed. Investment prioritization scenarios can be proposed for each of these sub-basins. The sub-basin that comes first (sub-basin 8) is given the top priority for developing the management plan to reduce surface runoff and soil erosion.

The results suggest that critical the sub-basins 8, 9, 2, 1, and 5 also represented areas with a high probability of landslide occurrence (Fig. 5). In order to reduce the sediment yield due to

surface soil erosion and shallow landslide disasters, these sub-basins were selected and recommended to implement management strategies with sub-basin 8 as the top potential priority.

SUMMARY

The study confirmed that the proposed physically-based distributed hydrological–geotechnical model could accurately simulate streamflow discharges, soil erosion, sediment yield, and the spatial pattern of documented historical landslides. From a basin-wide perspective, the study also demonstrated that not all the sub-basins in the study region make a significant contribution to the total sediment yield and shallow landslide occurrences. The model was able to identify the critical sub-basins, which are major contributors to sediment production. Future work will aim to link the model with algorithms representing various best management practice scenarios, and to assist in the design of control strategies for trapping and controlling sediment supply within the potential priority sub-basins.

Acknowledgements The support received from the International Consortium on Landslides (ICL) and the Disaster Prevention Research Institute (DPRI), Kyoto University, through the project "Asian Joint Research for Early Warning Technology of Landslides" is gratefully acknowledged. The authors would like to thank Dr Agung Bagiawan Ibrahim (Public Works Department of Indonesia) and Sumaryono (Geological Agency of Indonesia) for their help with providing the hydrological and landslide inventory database.

REFERENCES

Agus, F. & Wahyunto (2003) Evaluation of flood mitigation function of several land use systems in selected areas of west java, Indonesia. In: *Japan/OECD Expert Meeting on Land Conservation Indicators* (13–15 May, 2003, Kyoto, Japan).

Apip, Sayama, T., Tachikawa, Y. & Takara, K. (2010a) Spatial lumping of a distributed rainfall-sediment-runoff model and effective lumping scale. *Hydrological Processes* (accepted).

Apip, Takara, K, Yamashiki, Y., Ibrahim, A. B., Sassa, K. & Fukuoka, H. (2010b) A distributed hydrological–geotechnical model using satellite-derived rainfall for shallow landslide warning in a large basin. *Landslides Journal* **7**(3), 237–258.

Apip, Tachikawa, Y., Sayama, T., Takara, K. & Yamashiki, Y. (2010c) Assessing Sources of Parametric Uncertainty and Uncertainty Propagation in Sediment Runoff Simulations on Flooding. *J. Flood Risk Manage.* **3**, 270–284.

Borga, M., Fontana, G. D., Gregoretti, C. & Marchi, L. (2002) Assessment of shallow landsliding by using a physically based of hillslope stability. *Hydrol. Processes* **16**, 2833–2851.

Dickinson, W. T., Rudra, R. P. & Wall, G. J. (1990) Targeting remedial measures to control nonpoint source pollution. *Water Resour. Bull.* **26**(3), 499–507.

Foster, G. R. (1982) Modelling the erosion process. In: *Hydrologic Modelling of Small Basins.* American Society of Agricultural Engineers, St. Joseph, 295–380.

Huang, J. C. & Kao, S. J (2006) Optimal estimator for assessing landslide model performance. *Hydrol. Earth System Sci.* **10**, 957–965.

Lin, W. T., Tsai, J. S., Lin, C. Y. & Huang, P. H. (2008) Assessing reforestation placement and benefit for erosion control: A case study on the Chi-Jia-Wan Stream, Taiwan. *Ecol. Modelling* **211**, 444–452.

Montgomery, D. R. & Dietrich, W. E. (1994) A physically based model for the topographic control on shallow landsliding. *Water Resour. Res.* **30**, 1153–1171.

Tachikawa, Y., Nagatani, G. & Takara, K. (2004) Development of stage-discharge relationship equation incorporating saturated-unsaturated flow mechanism. *Ann. J. Hydraul. Engng* (*JSCE*) **48**, 7–12.

Takeuchi, K., Jayawardena, A. W. & Takahashi, Y. (eds) (1995) Catalogue of rivers for Southeast Asia and the Pacific — Volume I, The UNESCO-IHP Regional Steering Committee for Southeast Asia and the Pacific, UNESCO-IHP Publication, 103–114.

Yang, C. T. (1996) Total load transport. In: *Sediment Transport Theory and Practice*. McGraw Hill, USA, 141–210.